Topological superconductivity in proximitized double helical liquids

Chen-Hsuan Hsu

Institute of Physics, Academia Sinica, Taiwan

NCTS-iTHEMS Joint Workshop on Matters to Spacetime:
Symmetries and Geometry

Aug 29th, 2024

CHH, Nanoscale Horiz. DOI: D4NH00254G (2024); CHH et al., Phys. Rev. Lett. 121, 196801 (2018);
topical review: CHH et al., Semicond. Sci. Technol. 36, 123003 (2021)

Jelena Klinovaja (Univ Basel) & Daniel Loss (RIKEN & Univ Basel)

$$ National Science and Technology Council (NSTC), Institute of Physics & Academia Sinica, Taiwan

中央研究院 (Academia Sinica)

Main campus @Nangang, Taipei City

- 24 institutes, 8 research centers, ~1,100 faculty members

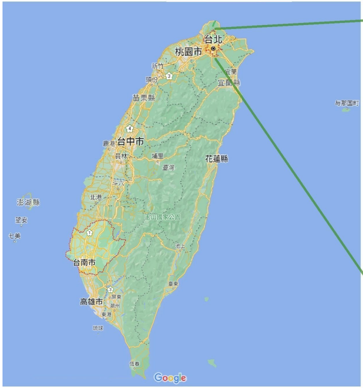

中央研究院

國立臺灣大學 National Taiwan University

Southern campus @Tainan City

- sustainable technology, quantum science, …

Notable Honorary Academicians:

- Leo Esaki, Tasuku Honjo, Shuji Nakamura, Ryoji Noyori, … etc.

Notable Academicians:

- Ta-You Wu former AS President (1983–1994)
  notable students: C. N. Yang and T.-D. Lee
- Maw-Kuen Wu (IoP faculty) & Paul C. W. Chu
  discovery of superconductivity with $T_c > 90$ K in the $YBa_2Cu_3O_{6+\delta}$ compound
- Yuan Tseh Lee former AS President (1994-2006)
  1986 Nobel Prize in Chemistry
- Chi-Huey Wong former AS President (2006-2016)
  2021 Welch Award in Chemistry
  2014 Wolf Prize in Chemistry

Welcome to visit us!

Outline

Introduction: Proximitized helical liquids as a platform for topological superconductivity

Interaction- and phonon-induced topological phase transitions in double helical liquids

Outline

Introduction: Proximitized helical liquids as a platform for topological superconductivity

Interaction- and phonon-induced topological phase transitions in double helical liquids

Helical edge channels in two-dimensional topological insulator (2DTI)

- Gapped 2D bulk and gapless 1D edges
- Topologically protected *helical edge channels* in time-reversal-invariant materials: electrons with opposite spins flow in the opposite directions

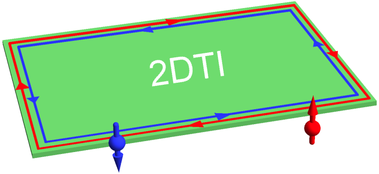

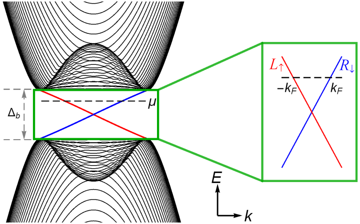

- Predictions and experimental realizations:
  - HgTe quantum wells Bernevig et al., Science 2006; Konig et al., Science 2007
  - InAs/GaSb heterostructures Liu et al., PRL 2008; Knez et al., PRL 2011
  - monolayer 1T′-WTe_2 Tang et al., Nat. Phys. 2017
  - bismuthene on SiC Reis et al., Science 2017
  - twisted bilayer $MoTe_2$ Kang et al., Nature 2024

  ⋮

Hinge channels in higher-order topological insulators (HOTI)

- Gapped bulk and surfaces in 3D 2nd-order topological insulator
- Surface gap changes its sign with the surface orientation
  $\Rightarrow$ surface-dependent Dirac mass: $m(\hat{n})$
  $\Rightarrow$ gapless states at the hinges between two surfaces with the opposite signs

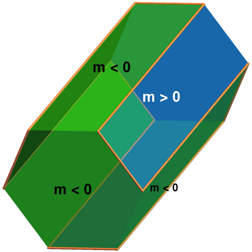

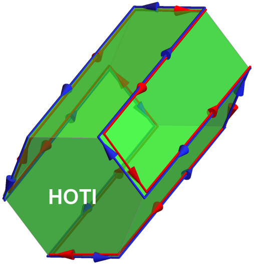

- Candidate materials:
  - Bi (theory/exp: Schindler et al., Nat. Phys. 2018; Murani et al., PRL 2019; Jäck et al., Science 2019)
  - Bi_4Br_4 (theory/exp: Noguchi et al., Nat. Mater. 2021)
  - multilayer WTe_2 in T_d structure (theory/exp: Choi et al., Nat. Mater. 2021)
  - SnTe, Bi_2TeI, BiSe, BiTe (theory: Schindler et al., Sci. Adv. 2018)

Helical liquid formed by interacting electrons in helical channels

- Electrons in 2DTI edges or HOTI hinges: $H_{\mathrm{hl}} = H_{\mathrm{kin}} + H_{\mathrm{ee}}$
- Kinetic energy term:

$$H_{\mathrm{kin}} = -i\hbar v_F \int dr \left(R_\downarrow^\dagger \partial_r R_\downarrow - L_\uparrow^\dagger \partial_r L_\uparrow \right)$$

- e-e interaction (g_2, g_4: interaction strength):

$$H_{\mathrm{ee}} = g_2 \int dr\, R_\downarrow^\dagger R_\downarrow L_\uparrow^\dagger L_\uparrow + \frac{g_4}{2} \int dr \left[\left(R_\downarrow^\dagger R_\downarrow \right)^2 + \left(L_\uparrow^\dagger L_\uparrow \right)^2 \right]$$

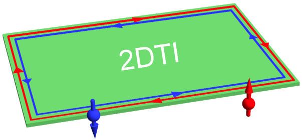

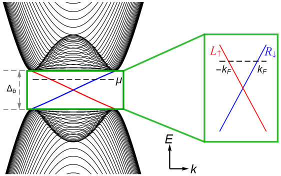

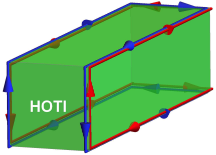

- 1D confinement geometry enhances interaction effects
  $\Rightarrow$ helical liquids: unconventional matters distinct from usual Fermi liquids in higher dimension

Nanoscale platforms for topological superconductivity

- Synthesizing nanoscale systems with nontrivial topology + superconductivity
- Proposals based on helical channels formed at 2DTI edges and HOTI hinges

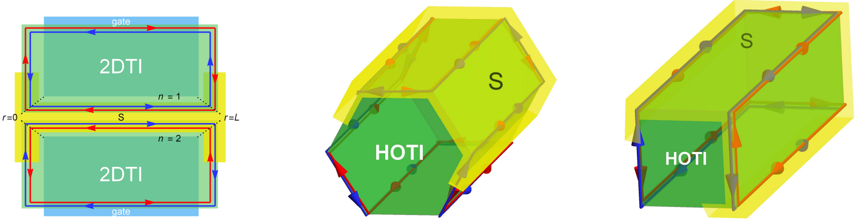

CHH et al., Semicond. Sci. Technol. 36, 123003 (2021)

- Proximity-induced pairing in helical channels
- When two helical channels are in contact with s-wave superconductor:
  Cooper pairs tunnel into the channel(s) while conserving momentum and spin
  $\Rightarrow$ two types of pairing: local and nonlocal

Proximity-induced pairing in helical channels

- local pairing or intrachannel pairing

- Pairing process in a single channel allowed by momentum and spin conservation

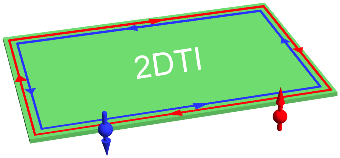

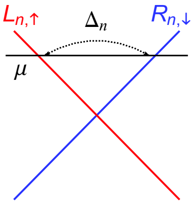

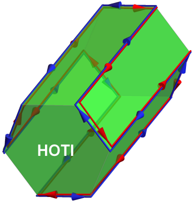

- Local pairing Δ_n (hinge index n):
  both Cooper-pair partners tunnel into the same channel

Proximity-induced pairing in helical channels

- nonlocal pairing or interchannel pairing

- Nonlocal (crossed Andreev) pairing:
  Cooper-pair partners tunnel into different channels

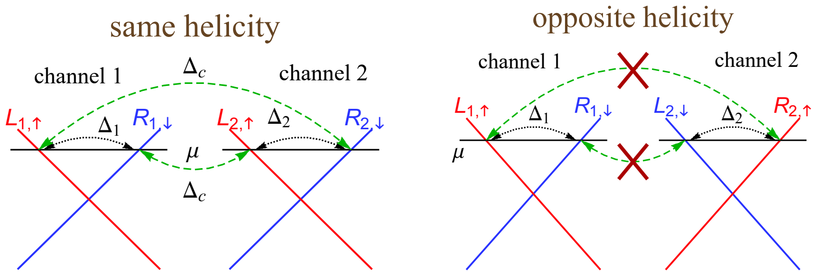

- Restriction due to momentum and spin conservation:
  nonzero pairing Δ_c allowed for two channels of the same helicity with the same μ

Proposals exploiting double helical liquids in 2DTI and HOTI

- Proximity effect allows nonlocal and local pairings in 2DTI/HOTI edges

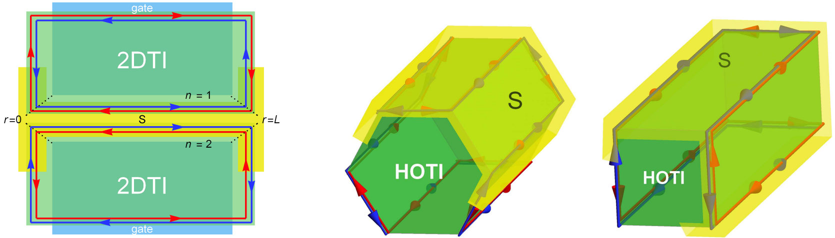

Klinovaja, Yacoby and Loss, PRB 90, 155447 (2014); CHH et al., Phys. Rev. Lett. 121, 196801 (2018)

- 2DTI setup: local gates required for adjusting local chemical potential $\mu_1 = \mu_2$
- HOTI setup: covering two side surfaces with a superconducting layer
- Local vs nonlocal pairings in two parallel helical channels
  $\Rightarrow$ competition between two gap opening mechanisms
- Band inversion takes place upon varying the relative strength of the local and nonlocal pairings

Criterion for Majorana zero mode (MZM) in proximitized HOTI and 2DTI

- Solving Bogoliubov-de Gennes equation in the single-particle description
  $\Rightarrow$ MZM solutions at zero energy satisfying self-conjugate property
- Band-inverted regime: Kramers pairs of MZM emerge at the corners of HOTI or 2DTI
- Topological criterion:
  $\Rightarrow$ nonlocal pairing dominates over local pairing

$$\Delta_{\mathrm{c}}^2 > \Delta_1 \Delta_2$$

- In noninteracting systems, local pairing prevails
  $\Rightarrow$ $\Delta_n > \Delta_{\mathrm{c}}$ in the absence of e-e interactions
  Reeg et al., PRB 2017
- Reversing the ratio of $\Delta_n / \Delta_{\mathrm{c}}$ through Coulomb interaction between electrons in the channels: the process where Cooper-pair partners tunnel into one channel costs higher energy than the process where they tunnel into different channels

MZM stabilized by intrachannel Coulomb interaction

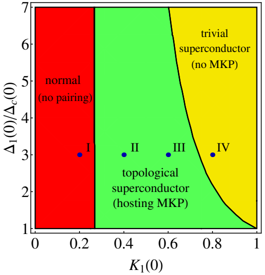

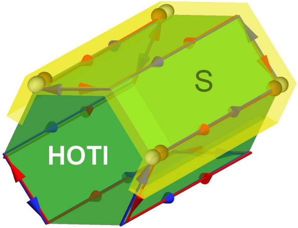

CHH et al., Phys. Rev. Lett. 121, 196801 (2018); CHH et al., Semicond. Sci. Technol. 36, 123003 (2021)

- Renormalization-group (RG) analysis to examine e-e interaction effects on Δ_n and Δ_c
- e-e interactions can stabilize MZM in double helical liquids
  $\Rightarrow$ suitable MZM platform *without magnetic fields and local voltage gates*
- Questions to be explored:
  - generality: topological criterion for generic interacting systems?
  - tunability: how to induce the transition between topological and trivial phases?
  - stability: how MZM survive under broader conditions (low-energy excitations)?

Outline

Introduction: Proximitized helical liquids as a platform for topological superconductivity

Interaction- and phonon-induced topological phase transitions in double helical liquids

Double helical liquids

- Helical liquids formed by interacting electrons in edge channels
  - bosonization:

$$R_{n,\downarrow}(r) = \frac{U_R}{\sqrt{2\pi a}} e^{i[-\phi_n(r)+\theta_n(r)]}, \quad L_{n,\uparrow}(r) = \frac{U_L}{\sqrt{2\pi a}} e^{i[\phi_n(r)+\theta_n(r)]}$$

- Double helical liquids:

$$H_{\mathrm{dh}} = \sum_{\delta\in\{s,a\}} \int dr\, \frac{\hbar u_\delta}{2\pi}\left[\frac{1}{K_\delta}\left(\partial_r\phi_\delta\right)^2 + K_\delta\left(\partial_r\theta_\delta\right)^2\right], \quad [\phi_\delta(r), \theta_{\delta'}(r')] = i\delta_{\delta\delta'}\frac{\pi}{2}\mathrm{sign}(r'-r)$$

  - interaction parameters $K_s,\ K_a$:

$$K_\delta = \left[1 + \frac{2}{\pi\hbar v_F}\left(U_{ee} + \delta V_{ee}\right)\right]^{-1/2}$$

  - $\delta \in \{s \equiv +,\ a \equiv -\}$: symmetric/antisymmetric combination of the two channels
  - U_{ee} (V_{ee}): intrachannel (interchannel) interaction strength
  - repulsive interaction: $U_{ee},\ V_{ee} > 0 \Rightarrow K_s \leqslant K_a \leqslant 1$

Proximity-induced pairings in double helical liquids

- Local (intrachannel) pairing:

$$
\begin{aligned}
V_{\mathrm{loc}} &= \int dr\, \frac{\Delta_1}{2}(R_1^\dagger L_1^\dagger - L_1^\dagger R_1^\dagger) + \frac{\Delta_2}{2}(R_2^\dagger L_2^\dagger - L_2^\dagger R_2^\dagger) + \mathrm{H.c.} \\
&= \int dr\, \frac{2\Delta_+}{\pi a} \cos(\sqrt{2}\theta_s)\cos(\sqrt{2}\theta_a) - \int dr\, \frac{2\Delta_-}{\pi a} \sin(\sqrt{2}\theta_s)\sin(\sqrt{2}\theta_a), \quad \Delta_\pm = (\Delta_1 \pm \Delta_2)/2
\end{aligned}
$$

- Nonlocal (interchannel) pairing:

$$
\begin{aligned}
V_{\mathrm{cap}} &= \int dr\, \frac{\Delta_{\mathrm{c}}(r)}{2} \left[(R_1^\dagger L_2^\dagger - L_2^\dagger R_1^\dagger) + (R_2^\dagger L_1^\dagger - L_1^\dagger R_2^\dagger)\right] + \mathrm{H.c.} \\
&= \int_0^L dr\, \frac{2\Delta_{\mathrm{c}}}{\pi a} \cos(\sqrt{2}\theta_s)\cos(\sqrt{2}\phi_a)
\end{aligned}
$$

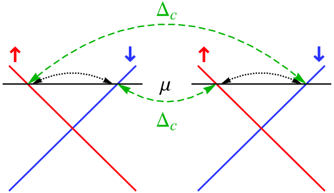

- Criterion for band inversion and topological phase (noninteracting limit):

$$
\Delta_{\mathrm{c}}^2 + \Delta_-^2 > \Delta_+^2
$$

  - identical pairing configuration $\Delta_- = 0$: dominant nonlocal pairing $\Delta_{\mathrm{c}} > \Delta_+$
  - here we revisit the topological criterion in interacting systems

Spin difference parity conservation of the pairing processes

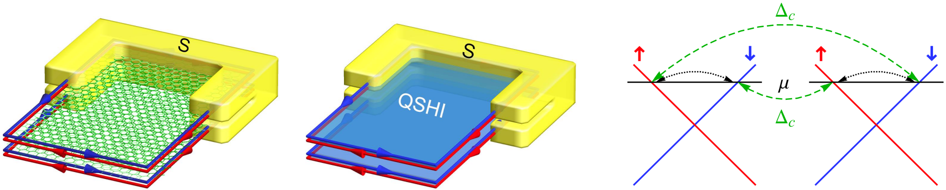

- Pairing processes in proximitized double helical liquids in the channels $n \in \{1, 2\}$
  - local pairing: $R^\dagger_{n,\downarrow} L^\dagger_{n,\uparrow} + \mathrm{H.c.} \quad \propto \Delta_+ \cos(\sqrt{2}\theta_s) \cos(\sqrt{2}\theta_a)$
  - nonlocal pairing: $R^\dagger_{1,\downarrow} L^\dagger_{2,\uparrow} + R^\dagger_{2,\downarrow} L^\dagger_{1,\uparrow} + \mathrm{H.c.} \quad \propto \Delta_c \cos(\sqrt{2}\theta_s) \cos(\sqrt{2}\phi_a)$
- Nonlocal pairing can change the spin difference between channels by two
  $\Rightarrow$ spin quantum number s_n not conserved for individual channel $n \in \{1, 2\}$
- Spin difference only changed by an even number
  $\Rightarrow$ conservation of “spin difference parity”: $(-1)^{s_1 - s_2}$

Ground-state degeneracy protected by the parity conservation

- Spin density $\propto \left(L^\dagger_{n,\uparrow}L_{n,\uparrow} - R^\dagger_{n,\downarrow}R_{n,\downarrow}\right) \propto \partial_r\theta_n$ for channel n
- Spin difference parity operator $P_{\rm sp}$ (θ_a field in the antisymmetric sector)

$$P_{\rm sp} \equiv (-1)^{s_1-s_2} = e^{-\sqrt{2}i\int dr\partial_r\theta_a}$$
$$\Rightarrow \quad P_{\rm sp}\phi_a P_{\rm sp}^{-1} = \phi_a - \sqrt{2}\pi$$

- From the compactness of ϕ_a field: $\phi_a \sim \phi_a \pm 2\sqrt{2}\pi$

$$P_{\rm sp}(\phi_a - \sqrt{2}\pi)P_{\rm sp}^{-1} = \phi_a - 2\sqrt{2}\pi \sim \phi_a$$

- Ground states for nonlocal pairing $\propto \cos(\sqrt{2}\phi_a)$ given by eigenstates of $P_{\rm sp}$:

$$|e/o\rangle_a = \frac{1}{\sqrt{2}}\Big(|\phi_a = \phi_0\rangle_a \pm |\phi_a = \phi_0 - \sqrt{2}\pi\rangle_a\Big), \qquad P_{\rm sp}|e/o\rangle_a = \pm|e/o\rangle_a$$

  - ground-state degeneracy protected by spin difference parity conservation

  $\Rightarrow$ nonlocal pairing term characterizes topologically nontrivial phase
- No degeneracy protected for local pairing $\propto \cos(\sqrt{2}\theta_a)$

Interaction effects on the phase diagram in the absence of phonons

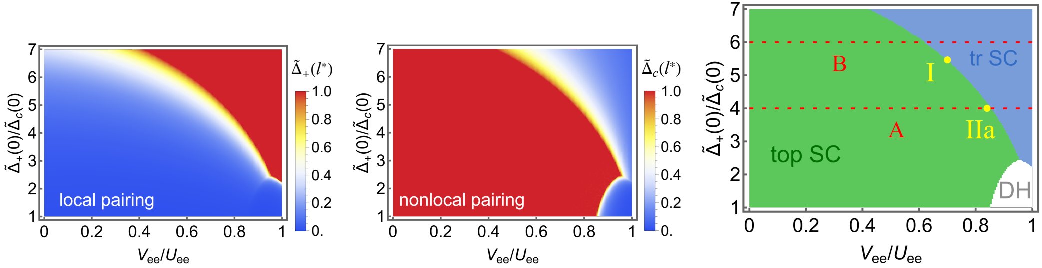

- Various phases: topological/trivial SC (top/tr SC) & double helical liquid (DH)
- Intrachannel interaction U_{ee} favors nonlocal pairing over local pairing: consistent with CHH et al., Phys. Rev. Lett. 121, 196801 (2018)
- Interchannel interaction V_{ee} reduces nonlocal pairing: sufficiently large V_{ee} induces phase transition towards trivial superconductivity $\Rightarrow$ suppressing topological zero modes
- Tunability provided by controlling the ratio of V_{ee}/U_{ee}

Electron-phonon-coupled system

- Phonon contribution to the Hamiltonian:

$$H_{\mathrm{ph}} + H_{\mathrm{ep}}$$

- Phonon subsystem:

$$H_{\mathrm{ph}} = \sum_n \int \frac{dr}{2\rho} \left[\pi_n^2 + \rho^2 c^2 \left(\partial_r d_n \right)^2 \right]$$

  - c: phonon velocity
  - ρ: mass density of lattice
  - d_n: displacement field due to phonons
  - π_n conjugate field of d_n

- Electron-phonon coupling (strength g): coupling of deformation potential to charge density

$$H_{\mathrm{ep}} = \sum_n g \int dr \, \left(\partial_r \phi_n \right) \left(\partial_r d_n \right)$$

- Phonons couple to ϕ field but not to θ field
  $\Rightarrow$ breakdown of self duality ($\phi \leftrightarrow \theta$, $K \leftrightarrow 1/K$)
- Previous perturbative analysis: phonons have no leading-order effects on helical liquids
  Budich et al., PRL 2012

Influence of electron-phonon coupling: excitation velocities

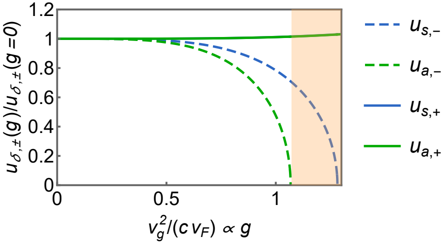

- Nonperturbative analysis on $H_{\mathrm{dh}} + H_{\mathrm{ph}} + H_{\mathrm{ep}}$
- Hybridization of electron and phonon modes leads to modifications of excitation velocity:

$$u_{\delta,\eta} = \sqrt{\frac{u_\delta^2 + c^2}{2} + \frac{\eta}{2}\sqrt{(u_\delta^2 - c^2)^2 + 4v_g^4}}, \text{ with } \delta \in \{s,a\}, \eta \in \{+,-\} \text{ and } v_g \propto g^{1/2}$$

$\Rightarrow$ quantifying how electron-phonon coupling alters excitation dynamics

- Phonon-induced modifications can be so significant that $u_{s/a,-} \to 0$
  $\Rightarrow$ Wentzel-Bardeen singularity Wentzel 1951; Bardeen 1951; Loss & Martin PRB 1994

Influence of electron-phonon coupling: scaling dimensions

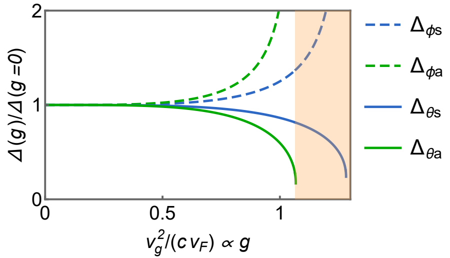

- Electron-phonon coupling $g \propto v_g^2$ influences the scaling dimensions of various operators
- Larger g values lower the scaling dimension of $e^{i\theta_\delta}$ and raise that of $e^{i\phi_\delta}$
  $\Rightarrow$ equivalent to attractive interactions
  $\Rightarrow$ enhancing both local and nonlocal pairings
- Electron-phonon coupling alters the scaling dimensions of pairing operators
  $\Rightarrow$ expecting effects on phase diagram through scaling dimensions

RG flow without phonons vs RG flow with phonons

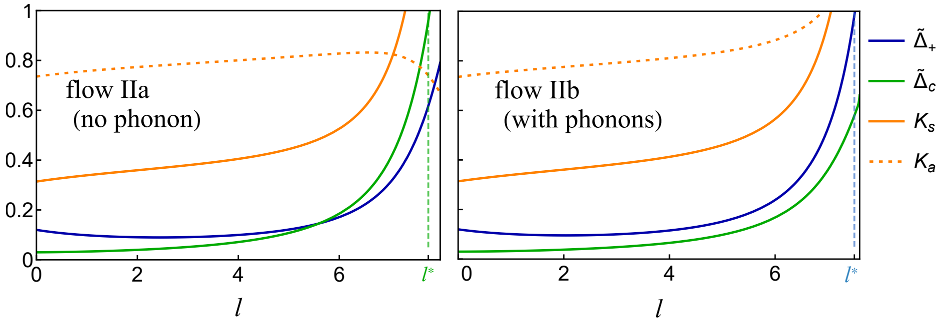

- Direct comparison of the RG flows: observing how phonons modify the flows
- Similar RG flows of K_s with and without phonons
  $\Rightarrow$ supporting both types of pairings
- Distinct behaviors in the RG flows of K_a: flowing to larger values with phonons
  $\Rightarrow$ favoring local over nonlocal pairing
- Opposite outcomes for topological properties despite identical initial parameters

Phonon-induced topological phase transition

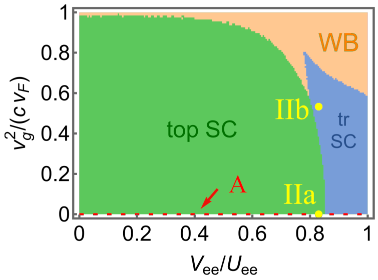

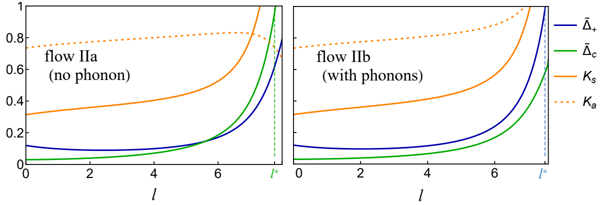

- Phase diagrams for a range of parameters $v_g^2/(cv_F) \propto g$ and V_{ee}/U_{ee}
- Phonons effectively mediate attractive interactions within each channel
  $\Rightarrow$ electron-phonon coupling enhances local pairing
- In terms of the RG flow, a nonzero v_g increases K_s and K_a
  $\Rightarrow$ enhancing $\tilde{\Delta}_n$ and suppressing $\tilde{\Delta}_c$
- Electron–phonon coupling can push the system from a topological phase to a trivial phase
- Reaching the WB singularity in a non-monotonic way

Electrically tunable topological phase transition

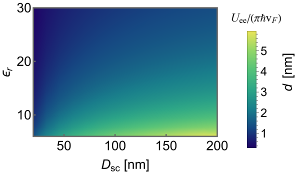

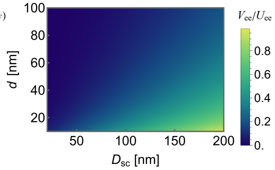

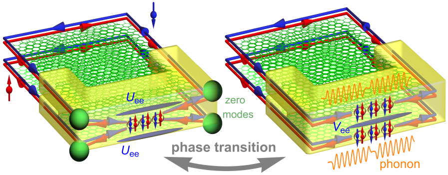

- Intrachannel interaction U_{ee}:
  tunable by screening length $D_{\rm sc}$ and dielectric constant ϵ_r of insulating layers
- Interchannel-to-intrachannel interaction strength ratio V_{ee}/U_{ee}:
  tunable by $D_{\rm sc}$, ϵ_r and interlayer separation d
- One can induce phase transitions by varying the strengths of U_{ee} and V_{ee}
  $\Rightarrow$ monitoring the presence/absence of topological zero modes
- Our results indicate electrically tunable topological phase transitions in double helical liquids

Conclusion

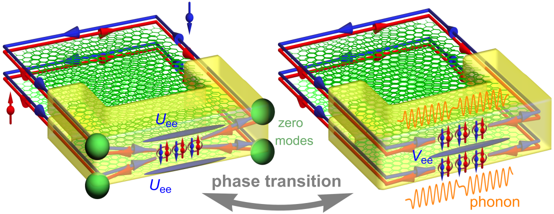

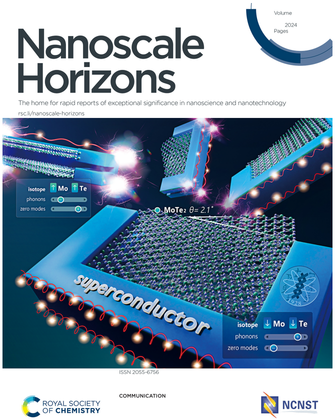

- Electrically tunable topological phase transitions
- Omnipresence of e-e interactions and phonons
  $\Rightarrow$ practical constraints in utilizing helical channels
  to realize topological zero modes

  CHH, Nanoscale Horiz. DOI：D4NH00254G (2024), in press;

  CHH et al., Phys. Rev. Lett. 121, 196801 (2018);

  topical review: CHH et al., Semicond. Sci. Technol. 36, 123003 (2021)
- Open positions in Condensed Matter Theory
  - https://sites.google.com/view/qmtheory
  - contact: chenhsuan@gate.sinica.edu.tw
  - welcome highly motivated postdocs, assistants and students!

Technical details

Nanoscale platforms for topological superconductivity

- Majorana zero modes (MZM) in nanoscale systems with nontrivial topology + superconductivity
- Intensively investigated setup in proximitized 1D wires with strong spin-orbit coupling

  Sato PLB 2003; Sato et al., PRL 2009; Sato & Fujimoto, PRB 2009; Lutchyn et al., PRL 2010; Oreg et al., PRL 2010 ...
  - typically chemical potential μ away from the Zeeman (partial) gap

    $\Rightarrow$ fine-tuning μ required
  - external magnetic field is necessary

    $\Rightarrow$ applying B field is detrimental to MZM
- Alternative setups proposed to avoid external B fields or fine-tuning μ
- Proposals based on helical channels formed at 2DTI edges and HOTI hinges

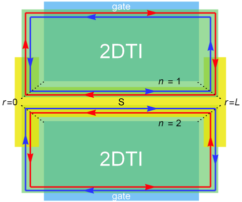

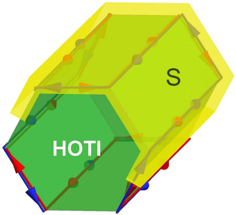

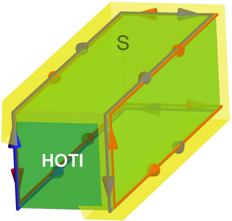

Self-duality point in the electronic subsystem

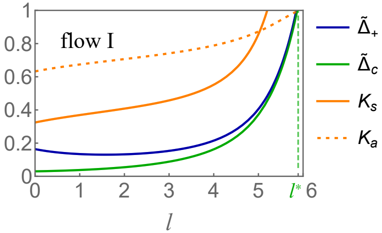

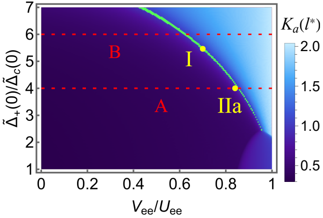

- Both local and nonlocal pairings tend to increase K_s, promoting ordering of θ_s
- Assuming ordering of θ_s, the low-energy model is governed by

$$V = \int \frac{dr}{a} \left[g_\phi \cos(\lambda_\phi \Phi) + g_\theta \cos(\lambda_\theta \Theta) \right], \quad \Phi = \frac{1}{\sqrt{\pi K_a}} \phi_a, \quad \Theta = \sqrt{\frac{K_a}{\pi}} \theta_a$$

$\Rightarrow$ self-dual sine-Gordon Hamiltonian (self-duality point: $K_a = 1$, $g_\phi = g_\theta$, $\lambda_\phi = \lambda_\theta$)

Lecheminant et al., Nucl. Phys. B 2002

- For certain initial parameters, RG flows tend to converge to $K_a \to 1$ and $g_\phi / g_\theta \to 1$
  $\Rightarrow$ a hierarchy of self-dual sine-Gordon model with different $\lambda_\phi, \lambda_\theta$ (fractional regime)

Total fermion parity conservation in proximitized double helical liquids

- With local and nonlocal pairing, the fermion number itself is not conserved
  $\Rightarrow$ the fermion number parity is conserved
- With the fermion number $q_{1,2}$ in channel $1, 2$, the total fermion parity operator can be defined

$$P_{\mathrm{f}} = (-1)^{q_1+q_2} = e^{-\sqrt{2}i \int dr \partial_r \phi_s}$$
$$\Rightarrow \quad P_{\mathrm{f}} \theta_s P_{\mathrm{f}}^{-1} = \theta_s - \sqrt{2}\pi$$

- From the compactness of θ_s field: $\theta_s \sim \theta_s \pm 2\sqrt{2}\pi$

$$P_{\mathrm{f}}(\theta_s - \sqrt{2}\pi) P_{\mathrm{f}}^{-1} = \theta_s - 2\sqrt{2}\pi \sim \theta_s$$

- The ground states for $\cos(\sqrt{2}\theta_s)$ are given by eigenstates of P_{f}: $P_{\mathrm{f}}|e/o\rangle_s = \pm|e/o\rangle_s$

$$|e/o\rangle_s = \frac{1}{\sqrt{2}}\Big(|\theta_s = \theta_0\rangle_s \pm |\theta_s = \theta_0 - \sqrt{2}\pi\rangle_s\Big)$$

RG flow analysis for with phonon contributions

- RG flow equations with the cutoff $a(l) = a(0)e^l$ and channel index $n \in \{1, 2\}$:

$$\begin{aligned}
\frac{d\tilde{\Delta}_+}{dl} &= \left[2 - \frac{1}{2}\sum_{\eta=\pm}\left(\frac{u_s\gamma^\theta_{s,\eta}}{K_s u_{s,\eta}} + \frac{u_a\gamma^\theta_{a,\eta}}{K_a u_{a,\eta}}\right)\right]\tilde{\Delta}_+ \\
\frac{d\tilde{\Delta}_c}{dl} &= \left[2 - \frac{1}{2}\sum_{\eta=\pm}\left(\frac{u_s\gamma^\theta_{s,\eta}}{K_s u_{s,\eta}} + \frac{u_a K_a\gamma^\phi_{a,\eta}}{u_{a,\eta}}\right)\right]\tilde{\Delta}_c \\
\frac{dK_s}{dl} &= 2\tilde{\Delta}_+^2 + 2\tilde{\Delta}_c^2 \\
\frac{dK_a}{dl} &= 2\tilde{\Delta}_+^2 - 2K_a^2\tilde{\Delta}_c^2
\end{aligned}$$

with $\tilde{\Delta}_+ = \Delta_+/\Delta_a$, $\tilde{\Delta}_c = \Delta_c/\Delta_a$, and ($\eta \in \{+,-\}$)

$$\gamma^\phi_{\delta,\eta} = \eta\left(\frac{u^2_{\delta,\eta} - c^2}{u^2_{\delta,+} - u^2_{\delta,-}}\right), \quad \gamma^\theta_{\delta,\eta} = \frac{\eta}{u^2_\delta}\left(\frac{u^2_\delta u^2_{\delta,\eta} - u^2_\delta c^2 + v^4_g}{u^2_{\delta,+} - u^2_{\delta,-}}\right)$$

More numerical analysis - I

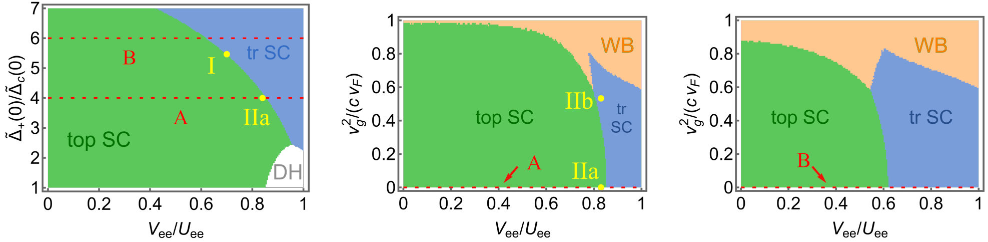

- Phase diagrams for different initial values of the local-to-nonlocal gap ratio $\tilde{\Delta}_n(0)/\tilde{\Delta}_\mathrm{c}(0)$

More numerical analysis - II

- Phase diagram without phonons for $U_{ee}/(\pi\hbar v_F) = 2$ and $\tilde{\Delta}_c(0) = 0.03$

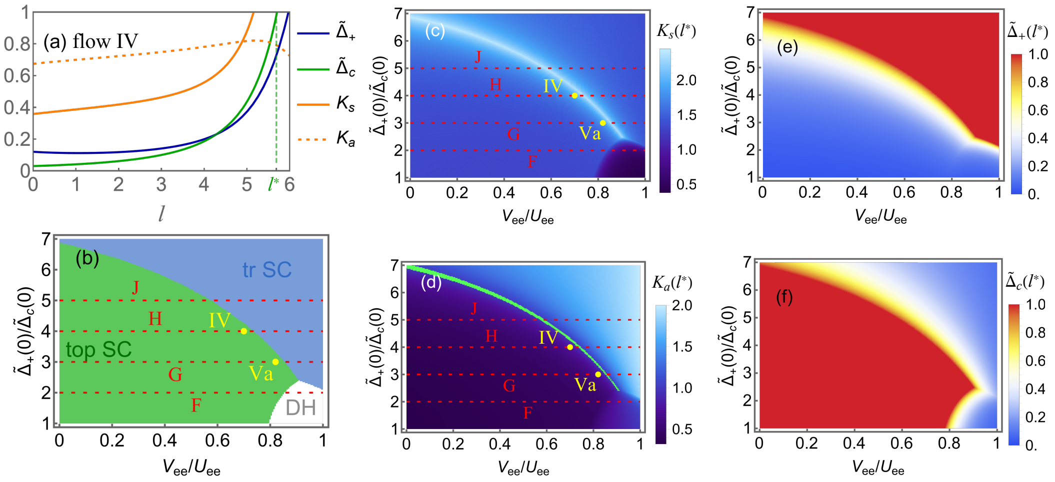

More numerical analysis - III

- RG flow and phase diagrams for $U_{ee}/(\pi\hbar v_F) = 2$ and $\tilde{\Delta}_c(0) = 0.03$

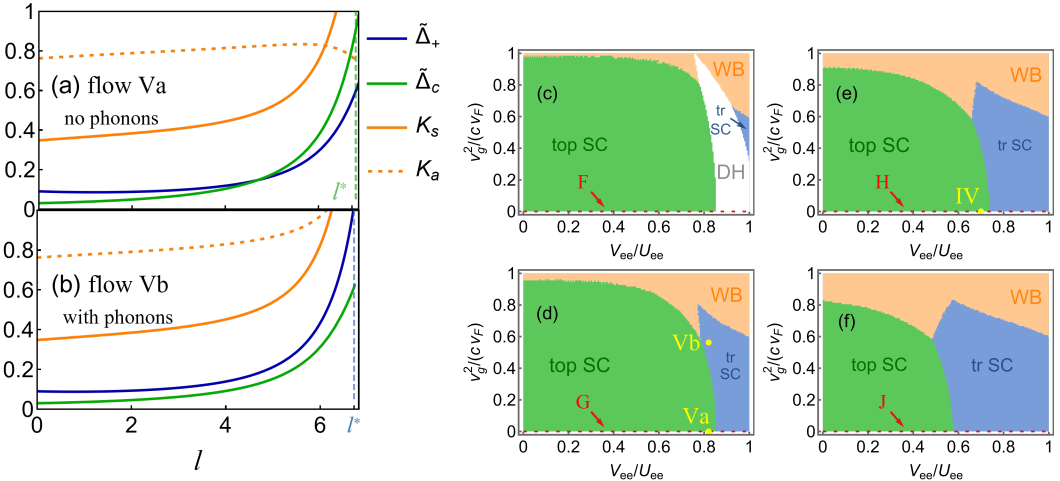

Appendix II

Backgrounds

No-go theorem in pure 1D systems

- No-go theorem:
  a single pair of helical states cannot be formed in pure 1D channels

continuous energy bands + Kramers degeneracy:

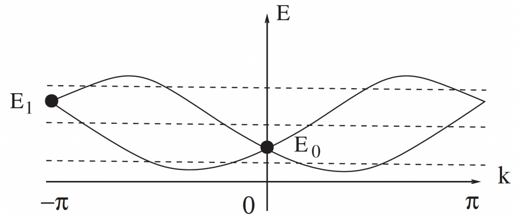

Wu et al., PRL 2006

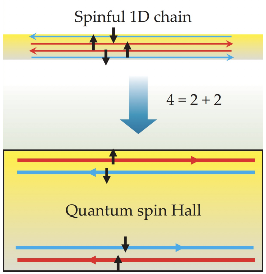

Qi et al., Phys. Today 2010

- No restriction for helical states in higher dimensions
  $\Rightarrow$ helical channels formed in 2D or 3D systems

Helical Tomonaga-Luttinger liquids

- Bosonization:

$$R_{\downarrow}(r) = \frac{U_R}{\sqrt{2\pi a}} e^{i[-\phi(r)+\theta(r)]}, \quad L_{\uparrow}(r) = \frac{U_L}{\sqrt{2\pi a}} e^{i[\phi(r)+\theta(r)]}$$

- *Helical Tomonaga-Luttinger liquid*:

$$H = \frac{\hbar u}{2\pi} \int dr \left[\frac{1}{K} \left(\partial_r \phi\right)^2 + K \left(\partial_r \theta\right)^2 \right], \quad [\phi(r), \theta(r')] = i\frac{\pi}{2} \mathrm{sign}(r' - r)$$

  - $K = 1$ for noninteracting systems; $K < 1$ for repulsive interaction

- Local density of states: universal scaling behavior

$$\rho_{\mathrm{dos}}(E, T) \quad \propto \quad T^{\alpha} \cosh\left(\frac{E}{2k_{\mathrm{B}}T}\right) \left| \Gamma\left(\frac{1+\alpha}{2} + i\frac{E}{2\pi k_{\mathrm{B}} T}\right) \right|^2$$

- Interaction parameter K can be extracted through $\alpha = (K + 1/K)/2 - 1$

Universal scaling behavior in spectroscopic measurements

- Scanning tunneling spectroscopy on bithmuthene on SiC:

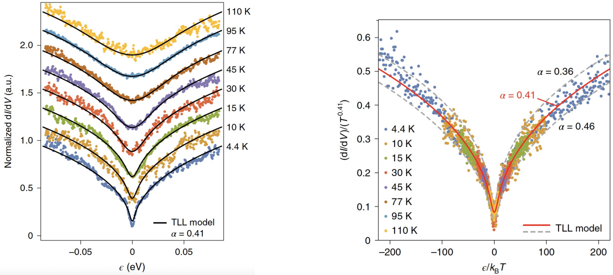

Stühler et al., Nat. Phys. 2020

$$\rho_{\mathrm{dos}}(E,T) \quad \propto \quad T^{\alpha}\cosh\left(\frac{E}{2k_{\mathrm{B}}T}\right)\left|\Gamma\left(\frac{1+\alpha}{2}+i\frac{E}{2\pi k_{\mathrm{B}}T}\right)\right|^{2}, \quad \alpha=\frac{K+1/K}{2}-1$$

- Experimental extracted value $K \approx 0.4 \Rightarrow$ strong e-e interaction
  $\Rightarrow$ suitable materials for topological zero modes

  CHH et al., Semicond. Sci. Technol. 36, 123003 (2021)

Identifying a B-field-free platform for double-wire setup

- B-field-free setup using double Rashba nanowires
  $\Rightarrow$ alternative requirement: sufficiently strong e-e interactions
  Klinovaja and Loss, PRB 2014; Thakurathi et al. PRB 2018
- Motivated to characterize e-e interaction strength in nanowires with strong SOC
- Universal scaling behavior of Tomonaga-Luttinger liquid in current-bias (I-V) curves
  $\Rightarrow$ developing an approach to deduce the e-e interaction strength in SOC nanowires
  CHH et al., Phys. Rev. B 100, 195423 (2019)
- Demonstrating strong e-e interactions in InAs wires
  $\Rightarrow$ a platform for MZM and parafermions without B field
  Sato, Matsuo, CHH et al., Phys. Rev. B 99, 155304 (2019)

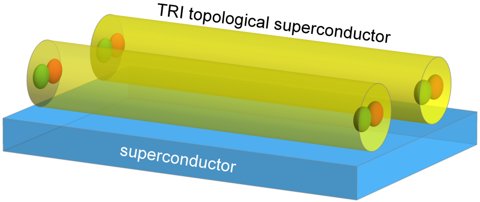

Experimental evidences for 1D gapless hinge states

- Experimental evidences for gapless hinge states in nanoscale systems:
  - bismuth (Bi) nanowires and bilayers

    Schindler et al., Nat. Phys. 2018; Drozdov et al., Nat. Phys. 2014; Murani et al., Nat. Commun. 2017; Murani et al., PRL 2019; Jäck et al., Science 2019
  - bismuth bromide (Bi_4Br_4)

    Noguchi et al., Nat. Mater. 2021

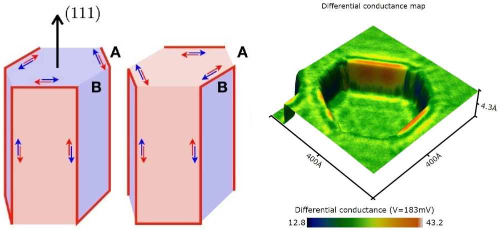

Schindler et al., Nat. Phys. 2018

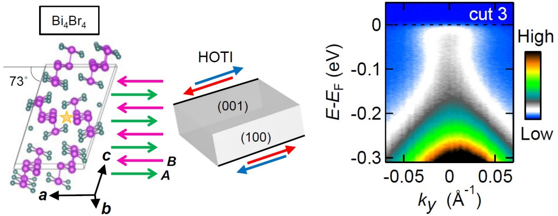

Noguchi et al., Nat. Mater. 2021

Edge transport in 2DTI samples

- $R_\downarrow$ and $L_\uparrow$ in helical channels:
  spin flip necessary for elastic backscattering $R_\downarrow \leftrightarrow L_\uparrow$
- Charge impurities:
  creating potential disorder $V_{\rm dis}$ but *no spin flip*: $\langle L_\uparrow | V_{\rm dis} | R_\downarrow \rangle = 0$
  $\Rightarrow$ (naive) expectation: no edge resistance and dissipationless transport

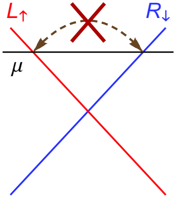

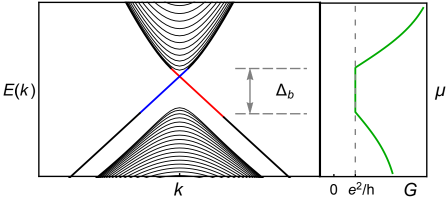

- Transport signature when the chemical potential μ is in the bulk gap $\Delta_{\rm b}$
  $\Rightarrow$ quantized edge conductance at e^2/h

Earlier experimental studies

- Experimental indication for charge transport via edge channels:

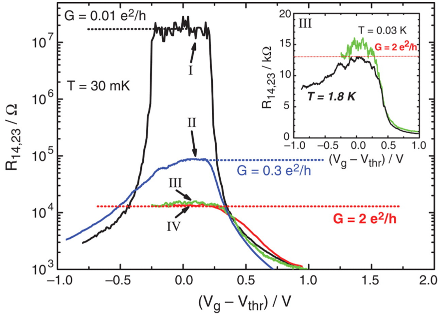

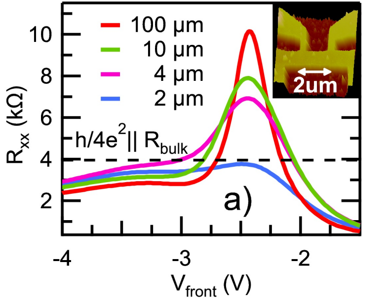

HgTe Konig et al., Science 2007

*logarithmic axis

InAs/GaSb Knez et al., PRL 2011

- Not well quantized conductance
  ⇒ motivation for subsequent works on edge transport

Finite edge resistance in realistic samples

- Experiments:
  no robust conductance quantization in larger samples
- Edge resistance scales with the edge length
  $\Rightarrow$ the presence of resistance sources

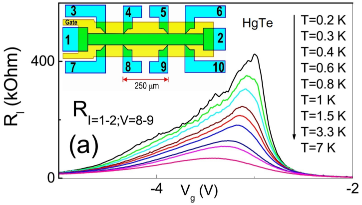

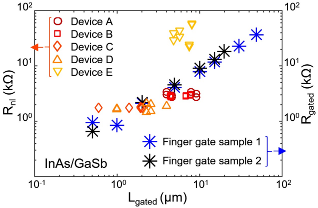

HgTe Olshanetsky et al., PRL 2015 InAs/GaSb Mueller et al., PRB 2017

- Various backscattering mechanisms proposed:
  time-reversal-symmetry breaking mechanisms or time-reversal-invariant (inelastic) processes

Time-reversal-symmetry breaking mechanisms

TRS breaking mechanism	R or $-\delta G$	Remark
Single magnetic impurity	$\begin{cases} T^{2K-2} & \text{for } T \ll T_{\mathrm{K}} \\ \text{const.} + \ln\left(\frac{\Delta_{\mathrm{b}}}{k_{\mathrm{B}}T}\right) & \text{for } T > T_{\mathrm{K}} \end{cases}$	
Single charge impurity (with a finite magnetic field)	T^{2K-2}	
Kondo lattice (1D Kondo array)	$\begin{cases} T^{-2} & \text{for } E_{\mathrm{pin}} < k_{\mathrm{B}}T \ll \Delta_{\mathrm{ka}}, \\ T^{2K-2} & \text{for } k_{\mathrm{B}}T > \Delta_{\mathrm{ka}} \end{cases}$	Localization at low T
Magnetic-impurity ensemble (with spin diffusion into the bulk)	$\begin{cases} e^{\Delta_{\mathrm{rs}}/(k_{\mathrm{B}}T)} & \text{for } T < T_{\mathrm{rs}} \\ T^{2K-2} & \text{for } T > T_{\mathrm{rs}} \end{cases}$	Localization for $K < 3/2$
Spiral-order-induced field (below spiral ordering T_{s})	$\begin{cases} m_{\mathrm{s}}^2 e^{\Delta_{\mathrm{sa}}/(k_{\mathrm{B}}T)} & \text{for } T < T_{\mathrm{sa}} \\ m_{\mathrm{s}}^2 T^{2K-2} & \text{for } T > T_{\mathrm{sa}} \end{cases}$	Localization for $K < 3/2$
Magnon (below spiral ordering T_{s})	$\begin{cases} \omega_{\mathrm{m}}^{2K-3} & \text{for magnon emission} \\ T^{3-2K} & \text{for magnon absorption} \end{cases}$	
DNP[f] (for $K \approx 1$ and finite spin-flip rate)	$(T + \text{const.})^{-1}$	
DNP with random SOI[g] (for $K \approx 1$ and long channels)	$T^{-2/3}$	

Topical review:

CHH et al., Semicond. Sci. Technol. 36, 123003 (2021)

Time-reversal-invariant mechanisms

TRS preserving mechanism	R or $-\delta G$
1PB by $H_{ee,5}$ (for clean systems)	$\begin{cases} e^{-\hbar v_F k_F/(k_B T)} & \text{for } k_B T \ll \hbar v_F k_F \\ T^{2K+3} & \text{for } k_B T \gg \hbar v_F k_F \end{cases}$
1PB by $H_{ee,5}$ & $H_{imp,f}$	T^{2K+2}
1PB by $H_{ee,5}$ & H_{imp}^{loc}	T^{2K+2}
1PB by $H_{ee,1}$ & $H_{imp,b}$	T^6 for $K \approx 1$
1PB by $H_{ee,3}$ & $H_{imp,b}$	T^4 for $K \approx 1$
2PB by $H_{ee,3}$ & $H_{imp,f}$	T^{8K-2} Localization for $K < 3/8$.
2PB by $H_{ee,3}$ & H_{imp}^{loc}	T^{8K-2}
Random SOI	0
Higher-order random SOI (single scatterer)	For $K > 1/2$: $\begin{cases} T^{4K} & \text{for } T < T^*_{rso} \\ T^{4K} \ln^2(k_B T/\Delta_b) & \text{for } T > T^*_{rso} \end{cases}$ For $1/4 < K < 1/2$: $\begin{cases} T^{8K-2} & \text{for } T < T^*_{rso} \\ T^{4K} \ln^2(k_B T/\Delta_b) & \text{for } T > T^*_{rso} \end{cases}$
1PB in charge puddles (for $K \approx 1$)	Short channel (a single puddle): even valley: $\begin{cases} T^4 & \text{for } k_B T \ll \delta_d \\ T^2 & \text{for } \delta_d \ll k_B T \ll E_{ch} \\ \text{const.} & \text{for } k_B T \gg E_{ch} \end{cases}$ even-odd transition: $\begin{cases} T^4 & \text{for } k_B T \ll \Gamma_t \\ \text{const.} & \text{for } \Gamma_t \ll k_B T \ll \delta_d \\ T^2 & \text{for } \delta_d \ll k_B T \ll E_{ch} \\ \text{const.} & \text{for } k_B T \gg E_{ch} \end{cases}$ odd valley: $\begin{cases} T^4 & \text{for } T \ll T_K \\ \ln^2(T/T_K) & \text{for } k_B T_K \ll k_B T \ll \delta_d \\ T^2 & \text{for } \delta_d \ll k_B T \ll E_{ch} \\ \text{const.} & \text{for } k_B T \gg E_{ch} \end{cases}$ Long channel: $E_{ch} \ll \delta_d$: T for $k_B T \ll \delta_d$ $E_{ch} \approx \delta_d$: $1/\ln^2[\delta_d/(k_B T)]$ for $k_B T \ll \delta_d$ $E_{ch} \gg \delta_d$: $\begin{cases} 1/\ln^2[\delta_d/(k_B T)] & \text{for } k_B T \ll \delta'_d \\ 1/\ln[\delta_d/(k_B T)] & \text{for } \delta'_d \ll k_B T \ll \delta_d \end{cases}$
Noise[j] (for $K \approx 1$, long channels)	Telegraph noise: $T^2 \tanh\left(\frac{E_{ch}}{2k_B T}\right)$ $1/f$ noise: $\begin{cases} T^2 & \text{for } k_B T \ll E_{ch} \\ T & \text{for } k_B T \gg E_{ch} \end{cases}$
Acoustic longitudinal phonon	0
Transverse phonon (for $K \approx 1$)	Short channel: $\begin{cases} e^{-\hbar v_F k_F/(k_B T)} & \text{for } k_B T \ll \hbar c_{ph,t} k_F \\ \text{const. } T^3 + \text{const. } T^5 & \text{for } k_B T \gg \hbar c_{ph,t} k_F \end{cases}$ Long channel: $\begin{cases} T^3 & \text{for } k_B T \ll \hbar v_F k_F,\ k_B \theta_D \\ T^5 & \text{for } \hbar v_F k_F \ll k_B T \ll k_B \theta_D \\ T & \text{for } k_B T \gg k_B \theta_D \gg \hbar v_F k_F \end{cases}$

Broken time-reversal symmetry by magnetic impurities

- Single magnetic impurity
  - isotropic coupling $J\mathbf{S}\cdot\mathbf{I} \Rightarrow$ spin-conserving terms: $S^zI^z,\ S^+I^-,\ S^-I^+$

  (x) strong-coupling regime: screened by Kondo effect

  Maciejko et al., PRL 2009

  (x) weak-coupling regime: polarization of the magnetic impurity

  $\Rightarrow$ unable to back scatter more electrons without additional depolarization mechanisms

  Tanaka et al., PRL 2011
  - spin-orbit-induced anisotropic coupling and non-spin-conserving terms: $S^yI^z,\ S^zI^y \cdots$

  Eriksson et al., PRB 2012

- Ensemble of magnetic impurities
  - 1D array of Kondo impurities with anisotropic coupling

    Altshuler et al., PRL 2013
  - dynamic nuclear spin polarization and spin-orbit interaction

    Lunde and Platero, PRB 2012; Del Maestro et al., PRB 2013
  - nuclear spins in host lattices (spin diffusion for depolarization)

    CHH et al., Phys. Rev. B 96, 081405(R) (2017); CHH et al., Phys. Rev. B 97, 125432 (2018)

Nuclear spins as resistance source in 2DTI edges

- Nuclear spins: typically present in 2DTI host lattices
  - InAs/GaSb: 100% of nuclei with nonzero spin
- Key ingredients in the mechanism:
  - broken time-reversal symmetry by nuclear spins
    $\Rightarrow$ allowing for spin-flip elastic backscattering
  - e-e interaction in 1D confinement
    $\Rightarrow$ enhancement of the backscattering effects
- Nuclear spins induce substantial resistance under realistic conditions (low T and long edges)

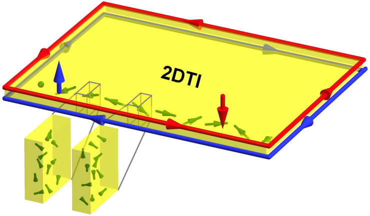

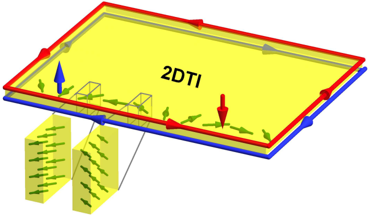

Interacting electrons in edge channels

- Spatial confinement enhances the influence of Coulomb interaction between electrons
  $\Rightarrow$ helical TLL formed in edge channels
- Bosonization:

$$R_{\downarrow}(r) = \frac{U_R}{\sqrt{2\pi a}} e^{ik_F r} e^{i[-\phi(r)+\theta(r)]}, \qquad L_{\uparrow}(r) = \frac{U_L}{\sqrt{2\pi a}} e^{-ik_F r} e^{i[\phi(r)+\theta(r)]}$$

- Kinetic energy and e-e interaction:

$$H_{\text{hTLL}} = H_0 + H_{\text{int}} = \int \frac{\hbar dr}{2\pi} \left\{ uK \left[\partial_r \theta(r)\right]^2 + \frac{u}{K} \left[\partial_r \phi(r)\right]^2 \right\}$$

  with the interaction parameter $K < 1$ and velocity u
- Hyperfine coupling between electron and nuclear spins:

$$\mathcal{H}_{\text{hf}} = \frac{A_0}{\rho_{\text{nuc}}} \sum_{n \in \text{nuclear spin}} \rho_{\text{el}}(\mathbf{x}_n) \frac{\boldsymbol{\sigma}}{2} \cdot \mathbf{I}_n$$

helical states

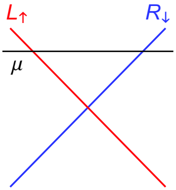

Edge transport in the disordered phase

- Randomly oriented nuclear spins:
  spin-flip elastic backscattering terms $R_\downarrow^\dagger L_\uparrow$ and $L_\uparrow^\dagger R_\downarrow$

$$\mathcal{H}_{\text{hf,b}} = \int \frac{dr}{2\pi a} V_{\text{hf}}(r) e^{2i\phi(r)} + \text{H.c.}$$

  with random potential V_{hf} induced by nuclear spins

- Backscattering action:

$$\frac{\delta \mathcal{S}_{\text{hf}}}{\hbar} = -\frac{D_{\text{hf}} u^2}{8\pi a^3} \int dr d\tau d\tau' \ \cos\left[2\phi(r,\tau) - 2\phi(r,\tau')\right]$$

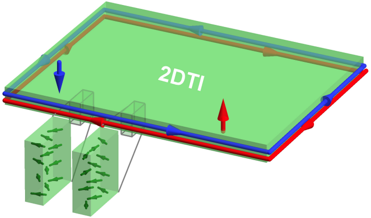

- Renormalization-group analysis on the relevance of $\delta\mathcal{S}_{\text{hf}}$
  $\Rightarrow$ edge resistance induced by disordered nuclear spins
- Gap opening for repulsive interaction
  $\Rightarrow$ localizationin a sufficiently long edge and sufficiently low temperature

Localization of edge states in the disordered nuclear spin phase

- Localization for a long edge $L > \xi_{\text{hf}}$ at low temperature $T < T_{\text{hf}}$

Physical parameter	InAs/GaSb	HgTe
Hyperfine coupling, A_0	50 μeV*	3 μeV*
Nuclear spin, I	3*	0.3*
Fermi velocity, v_F	4.6×10^4 m/s	5.1×10^5 m/s
Transverse decay length, a	9 nm	14 nm
Quantum well width, W_{QW}	15 nm	9 nm
Number of nuclei per cross section, $N_\perp$	3900	3200
Localization length ξ_{hf}**	17 μm	3.7 mm
Localization temperature T_{hf}***	100 mK	5.3 mK

* approximate average for all constituent isotopes

** localization length: $\xi_{\text{hf}} = aD_{\text{hf}}^{-1/(3-2K)}$

*** localization temperature: $T_{\text{hf}} = \hbar u/(k_B \xi_{\text{hf}})$

CHH et al., Phys. Rev. B 97, 125432 (2018)

- For InAs/GaSb, localization takes place in the experimentally accessible regime

Edge resistance due to disordered nuclear spins

- for InAs/GaSb, $K = 0.2$

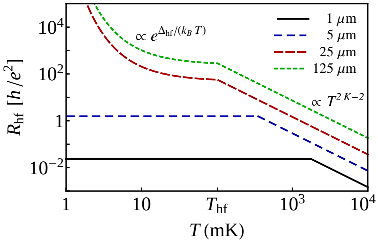

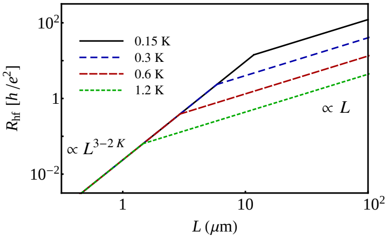

- Temperature dependence
  - high-T regime: fractional power law $R \propto T^{2K-2}$
  - low-T regime: exponential (long edge) or saturation (short edge)
  - localization-delocalization transition at $T_{\rm hf}$ for $L > \xi_{\rm hf}$
- Length dependence
  - long-edge regime: linear L dependence
  - short-edge regime: fractional power law $R \propto L^{3-2K}$

Nuclear spin order in Q1D channels

- Conduction electrons mediate RKKY coupling* between localized spins

$$\mathcal{H}_{\mathrm{hf}} \to \mathcal{H}_{\mathrm{RKKY}} = \sum_{i,j,\mu} \frac{J_{ij}^{\mu}}{N_{\perp}^{2}} \tilde{I}_i^{\mu} \tilde{I}_j^{\mu}$$

*Ruderman-Kittel-Kasuya-Yosida coupling

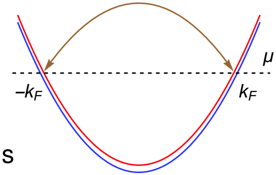

- RKKY-induced spin texture at low T in finite-size systems
  Braunecker et al., PRL 2009; Braunecker et al., PRB 2009
- Antiferromagnetic nuclear spin helix in ^{13}C nanotubes
  CHH et al., Phys. Rev. B 92, 235435 (2015)

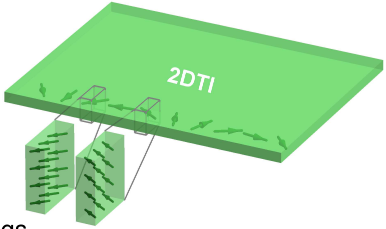

- RKKY coupling mediated by electrons in 2DTI edges
  $\Rightarrow$ spiral nuclear spin order for $T < T_0 \approx O(100\ \mathrm{mK})$
  in *finite-size* systems

- Additional processes in the ordered phase:
  spiral-field-assisted and magnon-mediated backscatterings

Spiral-field-assisted backscattering on impurities

- An effective field B_{Ov} created by the spiral order
  $\Rightarrow$ mixing $R_\downarrow$ and $L_\uparrow$ states
- Lifting topological protection of the edge states
  $\Rightarrow$ susceptible to charge impurities
- Spiral-field-assisted backscattering:

$$\mathcal{H}_{\mathrm{hx}} = \frac{1}{L}\sum_q V_{\mathrm{hx}} R_\downarrow^\dagger(q+2k_F)L_\uparrow(q) + \mathrm{H.c.}$$

  with $V_{\mathrm{hx}} \equiv B_{\mathrm{Ov}} V_{\mathrm{imp}}(4k_F)/(8\hbar v_F k_F)$
- Localization for $L > \xi_{\mathrm{hx}}$ and $T < T_{\mathrm{hx}},\ T_0$:

$$\xi_{\mathrm{hx}} = a D_{\mathrm{hx}}^{-1/(3-2K)}, \quad T_{\mathrm{hx}} = \hbar u D_{\mathrm{hx}}^{1/(3-2K)}/a$$

- Combination of spiral field and impurities $\Rightarrow$ exponential resistance below T_0

$$R_{\mathrm{hx}}(T) \propto R_0 \frac{\pi D_{\mathrm{hx}} L}{2K^2 a} e^{\Delta_{\mathrm{hx}}/(k_B T)}, \quad \Delta_{\mathrm{hx}} = \Delta_{\mathrm{b}} \left(2KD_{\mathrm{hx}}\right)^{1/(3-2K)}$$

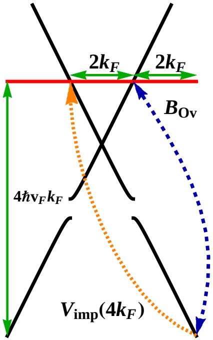

Magnon-mediated backscattering

- Backscattering and edge resistance due to magnon emission:

$$\frac{\delta\mathcal{S}^{\text{em}}_{\text{mag}}}{\hbar} = -\frac{D_{\text{mag}}u^2}{8\pi a^3}\int dr d\tau d\tau'\; e^{-\omega_{\text{mag}}|\tau-\tau'|}\left[1+n_B(\hbar\omega_{\text{mag}})\right]\cos\left[2\phi(r,\tau)-2\phi(r,\tau')\right]$$

$$R^{\text{em}}_{\text{mag}}(T) \propto R_0\frac{\pi D_{\text{mag}}L}{2K^2 a}\left[\frac{K\hbar\omega_{\text{mag}}(T)}{\Delta_{\text{b}}}\right]^{2K-3}$$

- Backscattering and edge resistance due to magnon absorption:

$$\frac{\delta\mathcal{S}^{\text{abs}}_{\text{mag}}}{\hbar} = -\frac{D_{\text{mag}}u^2}{8\pi a^3}\int dr d\tau d\tau'\; e^{\omega_{\text{mag}}|\tau-\tau'|}n_B(\hbar\omega_{\text{mag}})\cos\left[2\phi(r,\tau)-2\phi(r,\tau')\right]$$

$$R^{\text{abs}}_{\text{mag}}(T) \propto R_0\frac{\pi D_{\text{hf}}L}{2K^2 a}\left[1-m_{2k_F}(T)\right] \propto T^{3-2K}$$

- Strong dependence on magnon energy ($\hbar\omega_{\text{mag}}$ grows with $T\to 0$)
  - efficient for $\hbar\omega_{\text{mag}} \approx k_B T$ (i.e. $T \lesssim T_0$)
  - inefficient for $\hbar\omega_{\text{mag}} \gg k_B T$ (i.e. $T \to 0$)
- Both processes give power-law edge resistance of T, suppressed as $T\to 0$

Temperature dependence of the edge resistance

- summarizing all three backscattering mechanisms for InAs/GaSb, $K = 0.2$, $L = 25\ \mu$m

- Nonmonotonic T dependence: transport signature for the spiral order

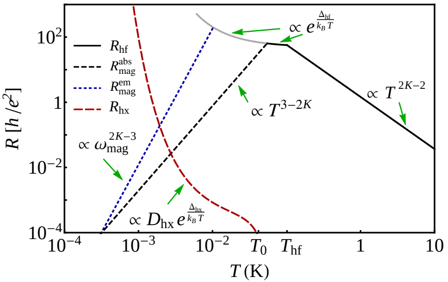

CHH et al., Phys. Rev. B 96, 081405(R) (2017)

- $T > T_0$ (disordered): power law for $T > T_{\rm hf}$
  exponential for $T < T_{\rm hf}$
- $T < T_0$ (sprial): power-law dependence for $T \lesssim T_0$ due to magnons
  $T \to 0$ divergence due to spiral-order-assisted backscattering on impurities

Edge transport of 2DTI

- Nuclear spins can lead to a substantial resistance in 2DTI edges
  - T, L, and V dependence: allowing future works to verify the proposed mechanisms

- Edge conductance suppressed in long samples at low temperatures
  $\Rightarrow$ fundamental limitation in scalable architectures
  CHH et al., Phys. Rev. B 96, 081405(R) (2017); CHH et al., Phys. Rev. B 97, 125432 (2018)

- Transport signatures for various mechanisms in the literature:
  - T dependence of edge resistance $R(T)$:
    - helical Tomonaga-Luttinger liquids: *fractional* power-law dependence
    - weakly interacting systems: *integer* power-law dependence

  - overall trend for $R(T)$ as $T \to 0$:
    - inelastic processes: $R \to 0$
    - broken time-reversal symmetry: nonvanishing R

  CHH et al., Semicond. Sci. Technol. 36, 123003 (2021)

Time-reversal-invariant mechanisms

- Kramers theorem:
  no overlap between wave functions of time-reversal pairs at the same energy
- No restriction for states at *different energies*
  $\Rightarrow$ inelastic processes
- Generic helical liquids in the presence of spin-orbit coupling
  $\Rightarrow$ right-moving $(+)$ and left-moving $(-)$ modes are no longer spin eigenstates

$$\begin{pmatrix} \psi_{\downarrow,q} \\ \psi_{\uparrow,q} \end{pmatrix} = U_{\rm so}(q) \begin{pmatrix} \psi_{+,q} \\ \psi_{-,q} \end{pmatrix}, \quad U_{\rm so}(q) = \begin{pmatrix} 1 & -q^2/k_{\rm so}^2 \\ q^2/k_{\rm so}^2 & 1 \end{pmatrix} + O(q^4)$$

- Density operator:

$$\rho_q = \sum_\sigma \sum_k \psi^\dagger_{\sigma,k}\psi_{\sigma,k+q} \to \sum_{\alpha\beta} [U^\dagger_{\rm so}(k) U_{\rm so}(k+q)]_{\alpha\beta} \psi^\dagger_{\alpha,k}\psi_{\beta,k+q}$$

- ρ_q affects the charge transport through e-e interaction and coupling to disorder
  Wu et al., PRL 2006; Xu and Moore, PRB 2006; Maciejko et al., PRL 2009; Schmidt et al., PRL 2012; Kainaris et al., PRB 2014; Ström et al., PRL 2010; Geissler et al., PRB 2014; Xie et al., PRL 2016; Kharitonov et al., PRB 2017 ...

Electron-electron interaction in generic helical liquids

$$
\begin{aligned}
H_{\text{ee}} &= \int dr dr' \, U_{\text{ee}}(r-r')\rho(r)\rho(r') \\
&\rightarrow \frac{1}{L}\sum_{qkp}\sum_{\alpha\alpha'\beta\beta'} U_{\text{ee},q}\psi^{\dagger}_{\alpha,k}\psi_{\beta,k+q}\psi^{\dagger}_{\alpha',p}\psi_{\beta',p-q}[U^{\dagger}_{\text{so}}(k)U_{\text{so}}(k+q)]_{\alpha\beta}[U^{\dagger}_{\text{so}}(p)U_{\text{so}}(p-q)]_{\alpha'\beta'}
\end{aligned}
$$

- Scattering processes:

$$
\begin{aligned}
H_{\text{ee},1} &= \frac{U_{\text{ee}}}{k_{\text{so}}^4 L}\sum_{qkp}\sum_{\alpha}(q^2+2qk)(q^2-2qp)\psi^{\dagger}_{\alpha,k}\psi^{\dagger}_{-\alpha,p}\psi_{-\alpha,k+q}\psi_{\alpha,p-q} \\
H_{\text{ee},2} &= \frac{U_{\text{ee}}}{L}\sum_{qkp}\sum_{\alpha}\psi^{\dagger}_{-\alpha,p}\psi^{\dagger}_{\alpha,k}\psi_{\alpha,k+q}\psi_{-\alpha,p-q} \\
H_{\text{ee},3} &= \frac{U_{\text{ee}}}{k_{\text{so}}^4 L}\sum_{qkp}\sum_{\alpha}(q^2+2qk)(q^2-2qp)\psi^{\dagger}_{\alpha,p}\psi^{\dagger}_{\alpha,k}\psi_{-\alpha,k+q}\psi_{-\alpha,p-q} \\
H_{\text{ee},4} &= \frac{U_{\text{ee}}}{L}\sum_{qkp}\sum_{\alpha}\psi^{\dagger}_{\alpha,p}\psi^{\dagger}_{\alpha,k}\psi_{\alpha,k+q}\psi_{\alpha,p-q} \\
H_{\text{ee},5} &= -\frac{2U_{\text{ee}}}{k_{\text{so}}^2 L}\sum_{qkp}\sum_{\alpha}\alpha(k^2-p^2)\psi^{\dagger}_{\alpha,k+q}\psi^{\dagger}_{-\alpha,p-q}\psi_{\alpha,p}\psi_{\alpha,k} + \text{H.c.}
\end{aligned}
$$

Disorder in generic helical liquids

- Coupling of charge density to the disorder potential

$$
\begin{aligned}
H_{\text{imp}} &= \int dr\, V_{\text{imp}}(r)\rho(r) \\
&\to \frac{1}{L}\sum_{qk} V_{\text{imp},q-k} \sum_{\alpha\beta} [U_{\text{so}}^{\dagger}(q)U_{\text{so}}(k)]_{\alpha\beta}\psi_{\alpha,q}^{\dagger}\psi_{\beta,k}
\end{aligned}
$$

- Forward and backward scattering processes:

$$
\begin{aligned}
H_{\text{imp,f}} &= \frac{V_{\text{imp}}}{L}\sum_{qk}\sum_{\alpha}\psi_{\alpha,q}^{\dagger}\psi_{\alpha,k} \\
H_{\text{imp,b}} &= \frac{V_{\text{imp}}}{L}\sum_{qk}\sum_{\alpha}\alpha\frac{q^2-k^2}{k_{\text{so}}^2}\psi_{\alpha,q}^{\dagger}\psi_{-\alpha,k}
\end{aligned}
$$

- Combination of H_{ee} and H_{imp}:
  various backscattering processes leading to finite edge resistance

Dominant processes allowed by momentum and energy conservation

- $H_{\mathrm{ee},1}$, $H_{\mathrm{ee},2}$, $H_{\mathrm{ee},4}$ conserve the numbers of right- and left-moving particles
  $\Rightarrow$ no direct effects on charge transport
- $H_{\mathrm{ee},5}$: backscattering of one particle + creation of a particle-hole pair (a,b)
- $H_{\mathrm{ee},3}$: backscattering of two particles (c)

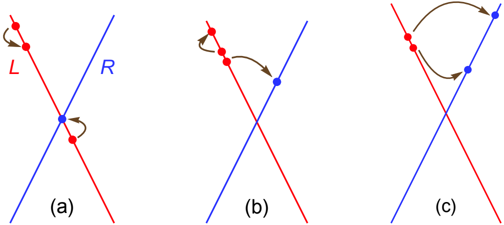

- Clean systems: $H_{\mathrm{ee},5}$ allowed when the Fermi level close to Dirac point $k_F \approx 0$ (a)
- Systems with disorder:
  compensation of the momentum differences
  $\Rightarrow$ 1PB by $H_{\mathrm{ee},5}$ and H_{imp} (b) and 2PB by $H_{\mathrm{ee},3}$ and H_{imp} (c)

  Kainaris et al., PRB 2014

Nomenclature for various time-reversal-invariant mechanisms

Reference	Notation or name in the original work
Kainaris *et al* (2014)	$g_1 \times b$ process
Wu *et al* (2006)	H_{dis} or two-particle backscattering due to quenched disorder
Xu and Moore (2006)	Scattering by spatially random quenched impurities
Kainaris *et al* (2014)	$g_3 \times f$ process (in their class of two-particle processes)
Schmidt *et al* (2012)	$H^{\mathrm{eff}}_{V,\mathrm{int}}$
Kainaris *et al* (2014)	$g_3 \times b$ process (in their class of one-particle processes)
Wu *et al* (2006)	H'_{bs} or impurity-induced two-particle correlated backscattering
Maciejko *et al* (2009)	H_2 or local impurity-induced two-particle backscattering
Lezmy *et al* (2012)	$g_{2\mathrm{p}}$ process or two-particle scattering
Schmidt *et al* (2012)	H_{int} or inelastic backscattering of a single electron with energy transfer to another particle-hole pair
Kainaris *et al* (2014)	g_5 process
Chou *et al* (2015)	$\hat{H}_W$ or one-particle spin-flip umklapp term
Kainaris *et al* (2014)	$g_5 \times f$ process (in their class of one-particle processes)
Chou *et al* (2015)	$\hat{H}_W$ (same notation for clean and disordered systems)
Kainaris *et al* (2014)	$g_5 \times b$ (in their class of one-particle processes)
Lezmy *et al* (2012)	g_{ie} process or inelastic scattering
Ström *et al* (2010)	H_R or randomly fluctuating Rashba spin–orbit coupling
Geissler *et al* (2014)	Random Rashba spin–orbit coupling
Kainaris *et al* (2014)	$g_{\mathrm{imp,b}}$ process
Xie *et al* (2016)	Random Rashba backscattering
Kharitonov *et al* (2017)	$\hat{H}_R$ or $U(1)$-asymmetric single-particle backscattering field
Crépin *et al* (2012)	Inelastic two-particle backscattering from a Rashba impurity

CHH et al., Semicond. Sci. Technol. 36, 123003 (2021)

Effective two-hinge system

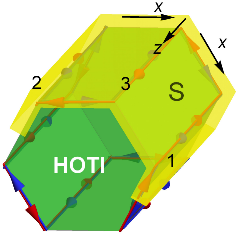

- Momentum and spin conservation + uniform μ:
  - ○ nonlocal pairing Δ_c between hinges 1&2
  - × nonlocal pairing between hinges 1&3 and 2&3

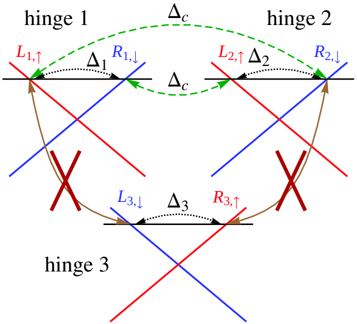

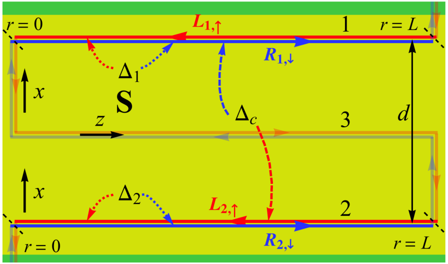

- In two hinges with the same helicity: competition between local & nonlocal pairings
- The middle hinge (labeled by 3) is decoupled from the other hinges (1 and 2)
  $\Rightarrow$ effective two-hinge system

MZM stabilized at the ends of the proximitized HOTI nanowire

- Nonlocal pairing allowed between long hinges, but suppressed between short hinges

$$\Delta_{\mathrm{c}}(r) = \begin{cases} \Delta_{\mathrm{c}}, & \text{for } 0 \leq r \leq L, \\ 0, & \text{otherwise}, \end{cases} \qquad \Delta_n(r) = \Delta_n$$

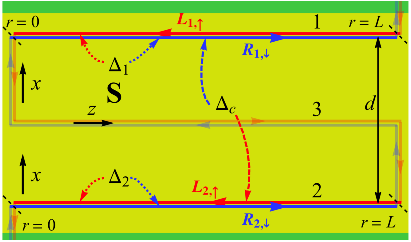

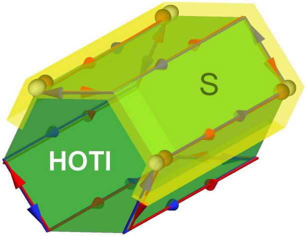

- System gap Δ_{b} changes its value *at the corners* where long hinges and short hinges meet
  $\Rightarrow$ inhomogeneous system gap
- We solve the Bogoliubov-de Gennes equation near one end of the system

Effective two-channel Hamiltonian for noninteracting systems

- Single-particle Hamiltonian: $H = H_0 + V_{\rm loc} + V_{\rm cap}$

$$\psi_n(r) = R_n(r)e^{ik_F r} + L_n(r)e^{-ik_F r}$$

  - right- and left-moving fields R_n and L_n for channel n (spin index suppressed)
  - kinetic energy:
$$H_0 = -i\hbar v_F \int dr\, \left(R_1^\dagger \partial_r R_1 - L_1^\dagger \partial_r L_1 + R_2^\dagger \partial_r R_2 - L_2^\dagger \partial_r L_2\right)$$
  - local pairing:
$$V_{\rm loc} = \int dr\, \left[\frac{\Delta_1(r)}{2}(R_1^\dagger L_1^\dagger - L_1^\dagger R_1^\dagger) + \frac{\Delta_2(r)}{2}(R_2^\dagger L_2^\dagger - L_2^\dagger R_2^\dagger) + \text{H.c.}\right]$$
  - nonlocal pairing:
$$V_{\rm cap} = \int dr\, \frac{\Delta_{\rm c}(r)}{2}\left[(R_1^\dagger L_2^\dagger - L_2^\dagger R_1^\dagger) + (R_2^\dagger L_1^\dagger - L_1^\dagger R_2^\dagger)\right] + \text{H.c.}$$

- In the basis $\Psi = (R_1, L_1, R_2, L_2, R_1^\dagger, L_1^\dagger, R_2^\dagger, L_2^\dagger)^{\rm T}$,

$$H = \frac{1}{2}\int dr\, \Psi^\dagger\left[-i\hbar v_F \eta^0\tau^0\sigma^z\partial_r - \Delta_+(r)\eta^y\tau^0\sigma^y - \Delta_-(r)\eta^y\tau^z\sigma^y - \Delta_{\rm c}(r)\eta^y\tau^x\sigma^y\right]\Psi$$

  - $\Delta_\pm(r) = [\Delta_1(r) \pm \Delta_2(r)]/2$
  - Pauli matrices for particle-hole (η^μ), channel (τ^μ), spin (σ^μ) space

Energy spectrum and band inversion

- Energy spectrum with uniform pairing gaps $\Delta_n(r) \to \Delta_n$ and $\Delta_c(r) \to \Delta_c$:

$$E^{(\pm,\pm)}(k) = \pm\left[(\hbar v_F k)^2 + \left(\Delta_+ \pm \sqrt{\Delta_-^2 + \Delta_c^2}\right)^2\right]^{1/2}$$

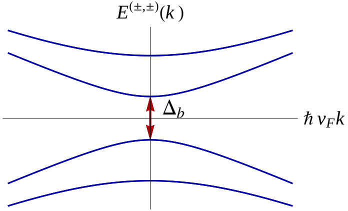

- System gap at $k = 0$:

$$\Delta_b \equiv E^{(+,-)}(k=0) - E^{(-,-)}(k=0) = 2\left(\Delta_+ - \sqrt{\Delta_-^2 + \Delta_c^2}\right)$$

- Δ_b changes its sign due to the competition between local and nonlocal pairing gaps $\Rightarrow$ *band inversion* occurs when $(\Delta_1\Delta_2 - \Delta_c^2)$ changes its sign
- Zero modes (bound states) for inhomogeneous Δ_b with sign change at some spatial point(s)

Kramers pairs of MZM and wave functions

- Single-particle Hamiltonian: $H = \frac{1}{2}\int dr\ \Psi^\dagger(r)\mathcal{H}(r)\Psi(r)$
- Bogoliubov-de Gennes equation at zero energy: $\mathcal{H}(r)\Phi_{\mathrm{mzm}}(r) = 0$
  $\Rightarrow$ solutions satisfying self-conjugate property and boundary condition at $r = 0$
  $\Rightarrow$ 2 MZM emerge for $\Delta_{\mathrm{c}}^2 > \Delta_1\Delta_2$
- 2 MZM solutions: $\Phi_{\mathrm{mzm},1}(r) = \Phi_>(r)\Theta(r) + \Phi_<(r)\Theta(-r)$ and $\Phi_{\mathrm{mzm},2} = \mathcal{T}\Phi_{\mathrm{mzm},1}$

$$\begin{aligned}\Phi_>(r) =& e^{-\kappa r} \times (i\eta, -\eta, -i, 1, -i\eta, -\eta, i, 1)^{\mathrm{T}},\\ \Phi_<(r) =& (i\eta e^{\kappa_1 r}, -\eta e^{\kappa_1 r}, -ie^{\kappa_2 r}, e^{\kappa_2 r}, -i\eta e^{\kappa_1 r}, -\eta e^{\kappa_1 r}, ie^{\kappa_2 r}, e^{\kappa_2 r})^{\mathrm{T}},\end{aligned}$$

with the step function $\Theta(r)$ and

$$\eta = \frac{\sqrt{\Delta_-^2 + \Delta_{\mathrm{c}}^2} - \Delta_-}{\Delta_{\mathrm{c}}},\ \kappa = \frac{\sqrt{\Delta_-^2 + \Delta_{\mathrm{c}}^2} - \Delta_+}{\hbar v_F},\ \kappa_1 = \frac{\Delta_1}{\hbar v_F},\ \kappa_2 = \frac{\Delta_2}{\hbar v_F}$$

- $\Phi_{\mathrm{mzm},1}$ & $\Phi_{\mathrm{mzm},2}$: Kramers pair of MZM protected by time-reversal symmetry
- Another pair of MZM near $r = L$: $\Phi_{\mathrm{mzm},1}$ and $\Phi_{\mathrm{mzm},2}$ with $r \to L - r$

Interacting helical channels

- Spatial confinement enhances the influence of Coulomb interaction between electrons
  $\Rightarrow$ helical Tomonaga-Luttinger liquids formed in the interacting helical channels
- Bosonization:
$$R_n(r) = \frac{U_R}{\sqrt{2\pi a}} e^{i[-\phi_n(r)+\theta_n(r)]}, \quad L_n(r) = \frac{U_L}{\sqrt{2\pi a}} e^{i[\phi_n(r)+\theta_n(r)]}$$
- Commutation relation of the bosonic fields:
$$[\phi_n(r), \partial_{r'}\theta_{n'}(r')] = i\pi\delta_{nn'}\delta(r-r')$$
- Kinetic energy and e-e interactions:
$$H_{\mathrm{el}} = H_0 + H_{\mathrm{int}} = \sum_{n=1,2} \int \frac{\hbar dr}{2\pi} \left\{ u_n K_n \left[\partial_r \theta_n(r)\right]^2 + \frac{u_n}{K_n} \left[\partial_r \phi_n(r)\right]^2 \right\},$$
  with the interaction parameter $K_n < 1$ for the hinge n and velocity $u_n = v_F/K_n$

Renormalized pairing gaps by e-e interactions

- RG analysis

- Local pairing:

$$H_{\mathrm{loc}} = \sum_{n=1,2} \frac{1}{\pi a} \int dr\, \Delta_n \cos[2\theta_n(r)]$$

- Nonlocal pairing:

$$H_{\mathrm{c}} = \frac{2}{\pi a} \int dr\, \Delta_{\mathrm{c}} \cos[\theta_1(r) + \theta_2(r)] \cos[\phi_1(r) - \phi_2(r)]$$

- Bosonic operators in H_{loc} and H_{c} do not commute
  $\Rightarrow$ *competing orders*

- We examine how the pairing gaps get renormalized by interactions through RG analysis

RG flow diagram in the absence of phonons

- RG flows for the initial values: $\Delta_1(0)/\Delta_c(0) = 3$, $a(0) = 5$ nm, and $L = 1$ μm

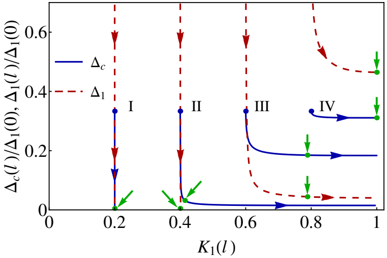

- Blue dots: initial points of $\Delta_c(0)$ for $K_1(0) = 0.2, 0.4, 0.6,$ and 0.8 (labeled by I, II, III, and IV)
- Green dots: renormalized pairing gaps at the end points of the RG flows
  $\Rightarrow$ adiabatically connected to $K = 1$ (refermionization)
- Local pairing gap suppressed more significantly than nonlocal pairing
- Renormalized pairings $\Delta_c(\ell^*) > \Delta_1(\ell^*)$ for RG flows II and III
  $\Rightarrow$ *moderate* interactions can reverse the relative strength of Δ_c and Δ_1

Microscopic model

- Tunnel Hamiltonian between the hinge states and a BCS superconductor:

$$H_{\mathrm{T}} = \sum_{n=1,2} \int dr d\mathbf{R} \left\{ t_n'(r,\mathbf{R}) \Big[R_n^\dagger(r) \psi_{\mathrm{s},\downarrow}(\mathbf{R}) + L_n^\dagger(r) \psi_{\mathrm{s},\uparrow}(\mathbf{R}) \Big] + \mathrm{H.c.} \right\}$$

- Weak tunnel amplitude t_n' (three-dimensional delta function):

$$t_n'(r,\mathbf{R}) \equiv t_n \delta(R_z - r)\delta(R_x - d_n)\delta(R_y),$$

  with $d_1 = d/2$, $d_2 = -d/2$, and the interhinge separation d

- BCS Hamiltonian (parent superconductor):

$$H_{\mathrm{BCS}} = \sum_{\mathbf{k},\sigma=\uparrow,\downarrow} \frac{\hbar^2(k^2 - k_{F\mathrm{s}}^2)}{2m_e} \psi_{\mathrm{s},\sigma}^\dagger(\mathbf{k}) \psi_{\mathrm{s},\sigma}(\mathbf{k}) + \Delta_{\mathrm{s}} \sum_{\mathbf{k}} \psi_{\mathrm{s},\uparrow}(\mathbf{k}) \psi_{\mathrm{s},\downarrow}(-\mathbf{k}) + \mathrm{H.c.}$$

- We first integrate out the field $\psi_{\mathrm{s},\sigma}$ in $H_{\mathrm{BCS}} + H_{\mathrm{T}}$ to obtain $\delta\mathcal{S}_{nn'} \propto t_n t_{n'}$
- We then construct the RG flow equations with the source terms depending on d and ξ_{s}

RG analysis from the microscopic model

- The RG flow equations read

$$
\begin{aligned}
\frac{d\tilde{t}_n(l)}{dl} &= \left[2 - \Big(K_n(l) + 1/K_n(l)\Big)/4\right] \tilde{t}_n(l), \\
\frac{d\tilde{\Delta}_n(l)}{dl} &= [2 - 1/K_n(l)]\, \tilde{\Delta}_n(l) + S_n(l)\tilde{t}_n^2(l), \\
\frac{d\tilde{\Delta}_c(l)}{dl} &= \left[2 - \frac{1}{4}\Big(K_1(l) + K_2(l) + 1/K_1(l) + 1/K_2(l)\Big)\right] \tilde{\Delta}_c(l) + S_c(l)\tilde{t}_1(l)\tilde{t}_2(l), \\
\frac{dK_n(l)}{dl} &= \tilde{\Delta}_n^2(l) + \frac{1}{2}\left[1 - K_n^2(l)\right] \tilde{\Delta}_c^2(l)
\end{aligned}
$$

- The source-term coefficients are given by

$$
\begin{aligned}
S_n(l) &= \frac{m_e v_{F\mathrm{s}}^2 L}{2\pi\Delta_\mathrm{s} a(l)} K_0\left(\frac{\Delta_\mathrm{s} a(l)}{\hbar u_n}\right), \\
S_\mathrm{c}(l) &= \frac{m_e v_{F\mathrm{s}}^2 L}{2\pi\Delta_\mathrm{s} d} e^{-d/\xi_s}\, |\sin(k_{F\mathrm{s}} d)|\, I_0\left(\frac{\Delta_\mathrm{s} a(l)}{2\hbar\sqrt{u_1 u_2}}\right) K_0\left(\frac{\Delta_\mathrm{s} a(l)}{2\hbar\sqrt{u_1 u_2}}\right)
\end{aligned}
$$

- Including the effects of the coherence length ξ_s and the interhinge separation d

RG analysis from the microscopic model (conti.)

- Superconducting gap $\Delta_s = 0.35$ meV and coherence length $\xi_s = 1.9\ \mu$m
- Interhinge separation: $d = 50$ nm (left) and $d = 100$ nm (right)

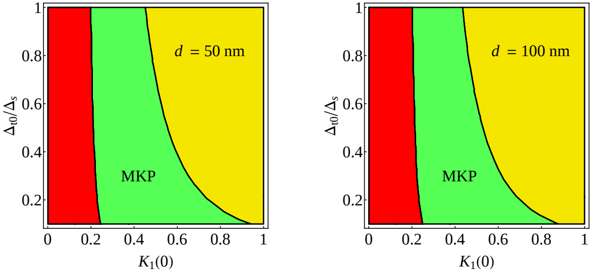

CHH et al., Semicond. Sci. Technol. 36, 123003 (2021)

- Consistent with the phase diagram from the effective-Hamiltonian model
- For $d \sim O(100\ \mathrm{nm})$ and $\xi_s \sim O(\mu\mathrm{m})$, we find a wide parameter range with MKPs
  $\Rightarrow$ aluminum as a suitable material for the proximity superconductor

Estimated value of the interaction parameter K_n

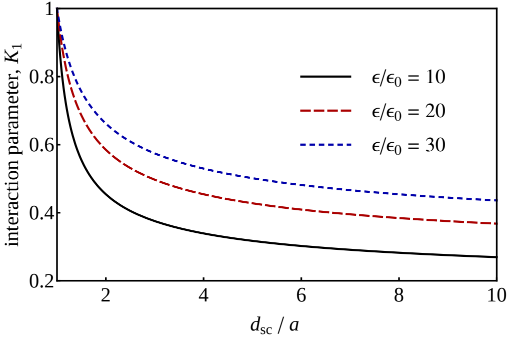

$$K_1 \approx K_2 = \left[1 + \frac{2e^2}{\pi^2 \epsilon \hbar v_F} \ln\left(\frac{d_{\mathrm{sc}}}{a}\right)\right]^{-1/2}$$

Maciejko et al., PRL 102, 256803 (2009)

- ϵ: dielectric constant, d_{sc}: screening length, v_F: Fermi velocity, a: hinge-state width
- Transverse decay length $a \approx 1$ nm from asymmetric SQUID experiment
  Schindler et al., Nat. Phys. 2018
- $v_F = 10^5$ m/s from $\Delta = \hbar v_F / a$, bulk gap $\Delta = O(0.1\ \mathrm{eV})$ from band-structure calculations
  Koroteev et al., PRB 2008; Wada et al., PRB 2011

Estimated bare gap ratio

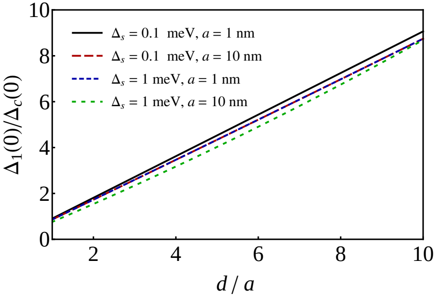

estimated from source-term approach:

$$\frac{\Delta_1(0)}{\Delta_c(0)} \approx \frac{d}{a} \frac{e^{d/\xi_s} K_0\left(\frac{\Delta_s a}{\hbar v_F}\right)}{K_0\left(\frac{\Delta_s a}{2\hbar v_F}\right) I_0\left(\frac{\Delta_s a}{2\hbar v_F}\right)}$$

- d: inter-hinge separation, v_F: Fermi velocity, a: hinge state width, I_0, K_0: modified Bessel functions, Δ_s, ξ_s: pairing gap and coherence length of the parent superconductor
- $\frac{\Delta_1(0)}{\Delta_c(0)}$ depends weakly on Δ_s and a (except for linear dependence on d/a)
- For $\Delta_s \in [0.1\ \mathrm{meV},\ 1\ \mathrm{meV}]$ and $a \in [1\ \mathrm{nm},\ 10\ \mathrm{nm}]$, $\Delta_1(0)/\Delta_c(0) \sim O(1)$–$O(10)$

Materials other than Bi nanowires

- helical hinge states

- Our proposed scheme can be applied to any 3D helical 2nd-order TIs
  $\Rightarrow$ the key is to bring two parahelical hinges into the proximity of a superconductor
- Our scheme can be applied to, but not limited to, Bi (111) nanowires
  - theoretically predicted helical HOTI materials: SnTe, Bi_2TeI, BiSe, and BiTe etc.
    Schindler et al., Sci. Adv. 2018
- While Bismuth is a bulk semimetal, trivial bulk states can be gapped by disorder or finite size

- Our RG analysis can also be applied to helical edge channels of 2DTIs
  (additional requirement: controlling μ of two isolated edge channels by local gates)

Proposals for MKP detection and quantum computing

Parity-controlled 2π Josephson effect

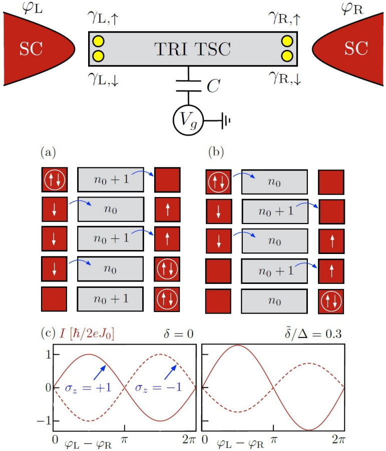

Schrade and Fu, PRL 120, 267002 (2018)

Majorana Kramers qubit

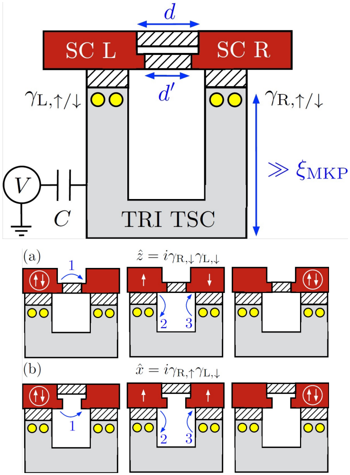

Schrade and Fu, PRL 129, 227002 (2022)